Journal of Heat Transfer

Technical Briefs

Technical Brief: Asymptotic Temperature Distribution in a Simulated Combustion Chamber

Anand B. Vyas
Visiting Assistant Professor
Department of Mathematical Sciences,
University of Delaware,
Newark, DE 19716

Joseph Majdalani[1]
Jack D. Whitfield Professor of High Speed Flows
Fellow ASME
Department of Mechanical, Aerospace, and
Biomedical Engineering,
University of Tennessee Space Institute,
Tullahoma, TN 37388
e-mail: drmajdalani@gmail.com

In an axisymmetric model of a solid rocket motor, a cylindrical combustion chamber with porous walls is considered. For a posited range of operating parameters, the energy equation is perturbed and linearized using the dimensionless Péclet number. The possibility of circumventing chemical reactions while retaining the essential physics of the problem is explored. This is accomplished by artificially introducing a distributed heat source above the propellant surface. The resulting energy equation is then solved to zeroth order. The analytical solution and corresponding temperature maps are verified qualitatively using comparisons with numerical simulations of the combustion chamber.
[DOI: 10.1115/1.2714591]

Keywords: asymptotic technique, thin sheet approximation, solid rocket motor, eigenfunction expansion

1 Introduction

Theoretical studies of aeroacoustic instability in solid rocket motors may be grouped under two categories: (1) those attempting to model unsteady combustion with limited emphasis on the internal flow details [1–6]; and (2) those attempting to describe the core flow details of a nonreactive mixture [7–11]. Over the years, both approaches have proven to be useful and complementary.

Exceptions to this classification exist and these can be illustrated in the resurging computational studies of Apte and Yang [12], Roh, Tseng and Yang [13], Roh and Culick [14], Venugopal et al. [15,16], and Vuillot and co-workers [17,18]. By focusing on numerical simulations, as opposed to analytical solutions of the internal flowfield, these studies have managed to combine the complex aeroacoustic interactions with the elements of combustion. Aside from these numerical studies, the intrinsic coupling between thermal and aeroacoustic modes has been often ignored in purely analytical studies.

In this work, we present a simple mathematical model that can couple the gas dynamics with the heat generated from propellant combustion. The model leads to a thermal solution of the flowfield that can mimic the effects of chemical reactions and entropy gradients that one normally associates with propellant combustion.

At first, the basic nature of the equations is examined. This enables us to identify small parameters that can be effectively used to simplify the model. The work is directed toward normalizing the energy equation by introducing a distributed heat source to replace the flame zone above the propellant surface. We ignore, at this stage, nonlinear heat radiation. Then, after providing estimates for various transport properties, we solve the ensuing equations using asymptotic expansions and compare our results to predictions made by other researchers.

2 Mathematical Model

As shown in Fig. 1, the coordinate system is so chosen that the longitudinal axis of the motor corresponds to the z axis. Due to symmetry, the domain of interest is reduced to $0 \leq r^* \leq R$, and $0 \leq z^* \leq L$. As usual, the internal radius of the cylindrical grain is denoted by R while the length of the grain is labeled L. A constant heat flux is imposed along the sidewall in a manner to account for the chemical reaction energy released during surface combustion.

The energy equation is written under the tacit assumptions that the flow is steady, incompressible, and axisymmetric with constant transport properties. Furthermore, we assume that the fluid enters the chamber at a uniform velocity V and that chemical reactions are confined to a thin sheet above the burning surface.

2.1 Governing Equation and Boundary Conditions. The energy equation under the stated assumptions can be expressed by

$$\rho c_p\left(u_r^*\frac{\partial T^*}{\partial r^*}+u_z^*\frac{\partial T^*}{\partial z^*}\right)-\left(u_r^*\frac{\partial p^*}{\partial r^*}+u_z^*\frac{\partial p^*}{\partial z^*}\right)$$
$$=\frac{k}{r^*}\frac{\partial}{\partial r^*}\left(r^*\frac{\partial T^*}{\partial r^*}\right)+k\frac{\partial^2 T^*}{\partial z^{*2}}+\dot{Q}^*$$
$$+2\mu\left[\frac{u_r^{*2}}{r^{*2}}+\left(\frac{\partial u_r^*}{\partial r^*}\right)^2+\left(\frac{\partial u_z^*}{\partial z^*}\right)^2+\frac{1}{2}\left(\frac{\partial u_z^*}{\partial r^*}\right)^2\right] \tag{1}$$

where the temperature boundary conditions correspond to

$$r^*=0,\quad \frac{\partial T^*}{\partial r^*}=0,\quad r^*=R,\quad T^*=T_w \tag{2}$$

[1]Corresponding author.

Contributed by the Heat Transfer Division of ASME for publication in the JOURNAL OF HEAT TRANSFER. Manuscript received February 5, 2006; final manuscript received July 17, 2006. Review conducted by Bengt Sunden.

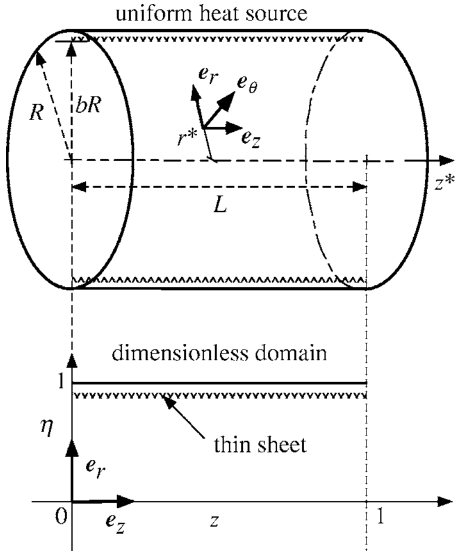

Fig. 1 Idealized motor chamber and system of coordinates illustrating the thin sheet approximation of the heat source

$$z^* = 0, \quad T^* = T_s, \quad z^* = L, \quad T^* = T_{ct} \tag{3}$$

Here T_w is the adiabatic flame temperature at the wall; T_s is the stagnation temperature at the head end; and T_{ct} refers to the throat condition at the downstream end. It is expedient to normalize Eqs. (1)–(3) using

$$r \equiv \frac{r^*}{R}; \quad z \equiv \frac{z^*}{L}; \quad u_r \equiv \frac{u_r^*}{V}; \quad u_z \equiv \frac{u_z^*}{V}; \quad p \equiv \frac{p^*}{\rho V^2}$$

$$\dot{Q} \equiv \frac{\dot{Q}^*}{\rho c_p (T_s - T_w)} \frac{R}{V} \tag{4}$$

and

$$T \equiv \frac{T^* - T_w}{T_s - T_w} \tag{5}$$

Following back substitution, the energy equation reduces to

$$u_r \frac{\partial T}{\partial r} + \phi u_z \frac{\partial T}{\partial z} - \mathrm{Ec}\left(u_r \frac{\partial p}{\partial r} + \phi u_z \frac{\partial p}{\partial z} \right) = \frac{1}{\mathrm{Pe}} \left[\frac{1}{r} \frac{\partial}{\partial r} \left(r \frac{\partial T}{\partial r} \right) + \phi^2 \frac{\partial^2 T}{\partial z^2} \right]$$
$$+ \dot{Q} + \frac{\mathrm{Ec}}{\mathrm{Re}} \left\{ 2 \left[\frac{u_r^2}{r^2} + \left(\frac{\partial u_r}{\partial r} \right)^2 + \left(\frac{\partial u_z}{\partial z} \right)^2 \right] + \left(\frac{\partial u_z}{\partial r} \right)^2 \right\} \tag{6}$$

where $\phi = R/L$ is the motor's aspect ratio and Re, Pr, Pe, and Ec symbolize the Reynolds, Prandtl, Péclet, and Eckert numbers. These are given by

$$\mathrm{Re} = \frac{VR}{\nu}; \quad \mathrm{Pr} = \frac{\mu c_p}{k}; \quad \mathrm{Pe} = \mathrm{Re}\,\mathrm{Pr}; \quad \mathrm{Ec} = \frac{V^2}{c_p (T_s - T_w)} \tag{7}$$

The normalized boundary conditions become

$$T(1,z) = 0; \quad \frac{\partial T(0,z)}{\partial r} = 0; \quad T(r,0) = 1; \quad T(r,1) = \hat{T} \tag{8}$$

where

$$\hat{T} = \frac{T_{ct} - T_w}{T_s - T_w}; \quad T_s = \frac{1}{2} T_{ct}(\gamma + 1); \quad \gamma = 1.4 \tag{9}$$

The last relation is due to the fundamental dependence of the static temperature on the stagnation temperature for choked conditions at the downstream end. It can be developed from $T_s = T[1 + (1/2)(\gamma - 1)M^2]$ for $M = 1$.

2.2 Dynamic Similarity Parameters. Given a gas mixture at 1000–3500 K and 10–100 bar, the dynamic viscosity is calculated to be 10^{-5}–10^{-4} N s/m^2. Then using Chung's correlation [19], the thermal conductivity is found to be approximately 2.0 W/m K. For the stated range of temperatures and pressures, one obtains a Prandtl number of order 10^{-2}. The Péclet number can hence vary from a small to a very large value. As the injection Reynolds number is varied from 10 to 10^6, the Péclet number changes from 10^{-1} to 10^4. In this study, we consider the case corresponding to the lower end of the injection rate, namely, to that of a small Péclet number.

In addition to the reciprocal of the Reynolds number, the problem exhibits another small parameter that can be used in the asymptotic work. Using average values of $V \approx 5$ m/s, $T_s \approx 3500$ K, $T_w \approx 700$ K, and $c_p \approx 1500$ J/kg K, it can be seen that the Eckert number in Eq. (7) is of order 6×10^{-6}. Being the ratio of kinetic and thermal energies, a small Eckert number corresponds to a setting in which thermal energy dominates over mean kinetic energy. This result is generally true inside a solid rocket motor (SRM) except for a small region near the nozzle throat. The assumption of Ec being small enables us to decouple the energy equation from the momentum equation. As evidenced by Eq. (6), both velocity and pressure become weak functions of temperature. This realization justifies the decoupling of thermal effects in some SRM core flow models such as those used by Culick [20], Vuillot [21], Casalis et al. [22], Couton et al. [23–25], and others.

Finally, in the interest of algebraic clarity, the present analysis is carried out for $\phi^2 = 1$. This assumption typifies aspect ratios used in upper stage rocket motors. The same approach may be repeated for $\phi^2 \ll 1$.

3 Small Péclet Number Solution

While the Eckert number remains the smallest perturbation quantity in Eq. (6), the Péclet number can be used either as a small, or a large parameter depending on the size of Re. In rocket motors, the large Pe injection combination is the more likely scenario. In this section, however, the small Péclet, moderate injection case is considered. Our solution extends over the range Re $\sim[10–100]$ that is of practical importance in some internal flow studies. In a recent core flow study carried out at the Center for Simulation of Advanced Rockets, an injection Reynolds number of 47.6 was used throughout the simulation [16].

3.1 Double Perturbation Expansions. Forthwith, one can multiply Eq. (6) by Pe and expand each variable in the two perturbation parameters, 1/Re and Pe. Next, terms of zeroth order in both perturbation parameters can be collected. One obtains the energy equation at zeroth order, namely

$$\frac{1}{r} \frac{\partial}{\partial r} \left(r \frac{\partial T^{(0,0)}}{\partial r} \right) + \frac{\partial^2 T^{(0,0)}}{\partial z^2} = -\dot{Q} \tag{10}$$

The first and second superscripts denote the order in 1/Re and Pe, respectively. Equation (10) is subject to the boundary conditions given by Eq. (8). Furthermore, it can be seen that the equation is linear and amenable to separation of variables. Using the method of superposition, a solution can be obtained and expressed in terms of eigenfunction expansions.

3.2 Eigenfunction Expansions. One may subdivide the temperature into three parts

$$T^{(0,0)} = T_1^{(0,0)} + T_2^{(0,0)} + T_3^{(0,0)} \tag{11}$$

This decomposition is deliberately pursued to facilitate the satisfaction of boundary conditions. Substitution into Eq. (10) gives rise to the following systems:

System 1

$$\frac{1}{r} \frac{\partial}{\partial r} \left(r \frac{\partial T_1^{(0,0)}}{\partial r} \right) + \frac{\partial^2 T_1^{(0,0)}}{\partial z^2} = 0$$

$$T_1^{(0,0)}(r,0)=1;\quad T_1^{(0,0)}(r,1)=0$$

$$T_1^{(0,0)}(1,z)=0;\quad \frac{\partial T_1^{(0,0)}(0,z)}{\partial r}=0 \tag{12}$$

System 2

$$\frac{1}{r}\frac{\partial}{\partial r}\left(r\frac{\partial T_2^{(0,0)}}{\partial r}\right)+\frac{\partial^2 T_2^{(0,0)}}{\partial z^2}=0$$

$$T_2^{(0,0)}(1,z)=0;\quad \frac{\partial T_2^{(0,0)}(0,z)}{\partial r}=0$$

$$T_2^{(0,0)}(r,0)=0;\quad T_2^{(0,0)}(r,1)=\hat{T} \tag{13}$$

and System 3

$$\frac{1}{r}\frac{\partial}{\partial r}\left(r\frac{\partial T_3^{(0,0)}}{\partial r}\right)+\frac{\partial^2 T_3^{(0,0)}}{\partial z^2}=-\dot{Q}$$

$$T_3^{(0,0)}(1,z)=0;\quad \frac{\partial T_3^{(0,0)}(0,z)}{\partial r}=0$$

$$T_3^{(0,0)}(r,0)=0;\quad T_3^{(0,0)}(r,1)=0 \tag{14}$$

Equations (12)–(14) consist of two Laplace equations with one nonhomogenous boundary condition, and one Poisson equation with homogenous boundary conditions. Their solution is described next.

3.3 Heat Source Addition. So far, we have only been concerned with the simplifications affecting the energy equation. The reaction energy released inside the combustion chamber is another ingredient that must be carefully evaluated. Since propellant physico-chemistry is not taken into consideration, the thermal energy release is distributed in the same manner that it is accounted for in basic two-dimensional models of premixed laminar flames (see Chu et al. [26], and Vyas et al. [27]). Here, we permit the heat to be delivered along a sheet above the propellant surface. This thin-sheet approximation is conveniently modeled using the Dirac delta function (see Fig. 1 for the tentative positioning of the heat source). Mathematically, this operation can be expressed by

$$\dot{Q}=\dot{q}(z)\,\delta(r-b) \tag{15}$$

where $\dot{q}(z)$ is the rate of heat generation that is allowed to vary along the chamber axis.

3.4 Leading Order Solution. Equations (12) and (13) can be solved using separation of variables and eigenfunction expansions. They can then be superimposed using Eq. (11) to construct the total solution at zeroth order in both perturbation variables. To start, we use

$$T_1^{(0,0)}(r,z)=\Phi(r)\Psi(z) \tag{16}$$

Substituting this product into Eq. (12), one gets

$$\frac{1}{\Phi}\frac{d^2\Phi}{dr^2}+\frac{1}{r}\frac{1}{\Phi}\frac{d\Phi}{dr}+\frac{1}{\Psi}\frac{d^2\Psi}{dz^2}=0 \tag{17}$$

with

$$\frac{d\Phi}{dr}(0)=0,\quad \Phi(1)=0,\quad \Psi(1)=0,\quad \Psi(0)=1 \tag{18}$$

At the outset, one obtains

$$T_1^{(0,0)}(r,z)=\sum_{n=1}^{\infty}K_n\sinh[\lambda_n(1-z)]J_0(\lambda_n r) \tag{19}$$

The nonhomogeneous boundary condition at $z=0$ can now be used to determine K_n. One finds

$$K_n=\frac{1}{\sinh(\lambda_n)}\frac{\int_0^1 rJ_0(\lambda_n r)dr}{\int_0^1 rJ_0^2(\lambda_n r)dr}=\frac{2}{\lambda_n J_1(\lambda_n r)\sinh(\lambda_n)} \tag{20}$$

Likewise, Eq. (13) can be solved to get

$$K_n=\frac{2\hat{T}}{\lambda_n J_1(\lambda_n r)\sinh(\lambda_n)} \tag{21}$$

Solutions of Eqs. (12) and (13) can be added to obtain

$$T_1^{(0,0)}+T_2^{(0,0)}=\sum_{n=1}^{\infty}\frac{2J_0(\lambda_n r)\{\sinh[\lambda_n(1-z)]+\hat{T}\sinh(\lambda_n z)\}}{\lambda_n\sinh(\lambda_n)J_1(\lambda_n r)} \tag{22}$$

Having reached a partial solution, one may solve the remaining system given by Eq. (14). One retrieves

$$T_3^{(0,0)}=\sum_{n=1}^{\infty}\sum_{m=1}^{\infty}B_{mn}\sin(m\pi z)J_0(\lambda_n r) \tag{23}$$

Expanding Eq. (15) and using the orthogonality of eigenfunctions, one determines the double eigenfunction expansion coefficients. These are

$$\dot{q}(z)\,\delta(r-b)=\sum_{n=1}^{\infty}\sum_{m=1}^{\infty}A_{mn}\sin(m\pi z)J_0(\lambda_n r) \tag{24}$$

and so

$$A_{mn}=\frac{\int_0^1\int_0^1\dot{q}(z)\,\delta(r-b)\sin(m\pi z)J_0(\lambda_n r)r\,dr\,dz}{\int_0^1\int_0^1\sin^2(m\pi z)J_0^2(\lambda_n r)r\,dr\,dz}=\frac{4J_0(\lambda_n b)}{J_1^2(\lambda_n)}\int_0^1\int_0^1\dot{q}(z)\sin(m\pi z)dz \tag{25}$$

By substituting Eq. (23) into the left-handside of Eq. (14), it is possible to determine the A_{mn} coefficients by relating Eq. (23) to the double expansion coefficients of Eq. (25). One gets

$$B_{mn}=\frac{A_{mn}}{m^2\pi^2+\lambda_n^2} \tag{26}$$

This completes our leading-order solution in both perturbation parameters. We now have

$$T^{(0,0)}=\sum_{n=1}^{\infty}\frac{2J_0(\lambda_n r)\{\sinh[\lambda_n(1-z)]+\hat{T}\sinh(\lambda_n z)\}}{\lambda_n\sinh(\lambda_n)J_1(\lambda_n r)}+\sum_{n=1}^{\infty}\sum_{m=1}^{\infty}B_{mn}\sin(m\pi z)J_0(\lambda_n r) \tag{27}$$

4 Results

To better understand the solution behavior, we have plotted the constant temperature contour maps derived from $T^{(0,0)}$. The heat source is distributed along a thin sheet located at a radial distance of $b=0.9$. We have chosen a spatially uniform heat generation in accordance with the standard thin sheet approximation. This may be justifiable insofar as averaging of unsteady flame variations over time yields a constant flame profile. We have considered three separate cases characterized by three orders of magnitude variations in the heat generation rate.

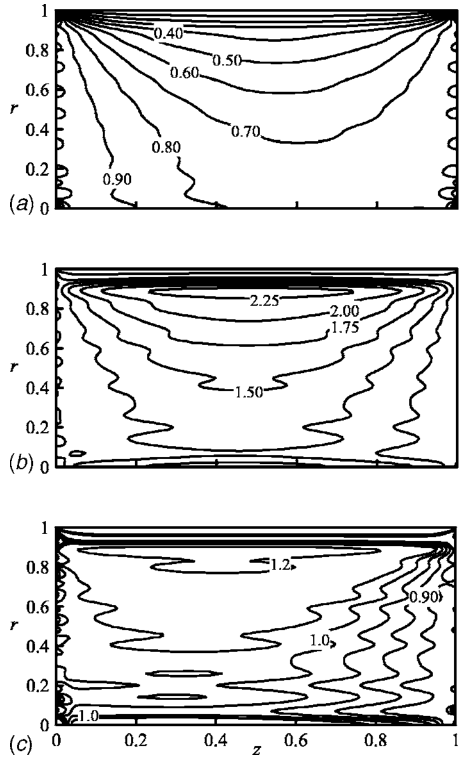

Fig. 2 Isotherms for $b=0.9$, $\hat{T}=0.8$, and (a) $\dot{q}=2.5$; (b) $\dot{q}=25$; and (c) $\dot{q}=12.5$

4.1 Case 1: $b=0.9$, $\hat{T}=0.8$, and $\dot{q}=2.5$. For a sufficiently low heat generation rate, we observe in Fig. 2(*a*) a linear temperature gradient that increases away from the wall. Since the maximum temperature occurs at the core, the solution with low heat input does not appear to be a suitable model of the flame zone. The reason can be attributed to the heat generation term being of the same order as the diffusive term. Note that the temperature variations along the boundaries are due to the asymmetric boundary conditions. The small fluctuations in the corresponding isotherms are due to the finite number of eigenvalues used in our code. Presently, we have used only 25 eigenvalues in the radial and axial directions. By carrying out a sensitivity analysis, we have found that further increases in the number of eigenvalues (e.g., to 30) do not affect the solution in the core. The small temperature variations along the boundaries, however, must be tolerated. It can be verified that the average values of these deviations over the radial and longitudinal lengths add up to the prescribed boundary values. The justification for $\hat{T}=0.8$ is based on Eq. (9). Since our analysis has indicated that the value of $\hat{T}$ varies between 0.77 and 0.8, the upper limit has been chosen. The skewed thermal contours in the downstream direction can be attributed to the relatively weak heat source. The slow variation in the temperature near the surface leads to a shallow temperature gradient that does not conform to temperature predictions in rocket motors. This rate of heat release is clearly not sufficient to reproduce the desired thermal field.

4.2 Case 2: $b=0.9$, $\hat{T}=0.8$, and $\dot{q}=25$. To better simulate rocket motor conditions, the heat source is first increased by one order of magnitude. As shown in Fig. 2(*b*), it can be seen that, for a large heat generation rate, a steeper gradient in temperature is obtained that can mimic the temperature gradient between the burning surface and the flame inside a solid rocket motor. The nearly symmetric temperature map is the outcome of a dominant heat source and a weak convective motion. Also, the intense heat generation near $r=0.9$ roughly approximates the mechanism of heat generation associated with a laminar premixed flame. However, by comparing the magnitude of the normalized temperature distribution to that obtained in a solid rocket motor, we realize that the observed distribution overestimates the maximum temperature in an actual motor. Since our normalized peak temperature of 2.2 corresponds to about 5000 K, it constitutes a modest exaggeration of practical values. In rockets, one expects this temperature to fall in the vicinity of 3500 K. Given that the imposed heat distribution rate is not derived from experimental data, it can be adjusted in a manner to produce more realistic temperature maps. We conclude that a more appropriate value for artificial heat generation should be used, namely, one that is closer to 12. When such a level is imposed, the thermal maps become a more adequate representation of the temperature field in a typical motor. This case is illustrated in Fig. 2(*c*). Therein, the weak temperature variation in the axial direction can be attributed to the weak injection-driven flow effect in relative proportion to the thermal heat dispersion effect. The rapid temperature variation near the wall is also consistent with the steep thermal gradients observed in rockets. Our analytical results appear to be in qualitative agreement with the numerical findings of Roh et al. [28] (cf. Fig. 2, p. 894).

5 Conclusions

An asymptotic investigation is carried out to estimate the transport properties and physical quantities arising in the energy equation applied to a simulated solid rocket motor chamber. The study reveals the presence of three contributing parameters. These are the Eckert number, the injection Reynolds number, and the Péclet number. The Eckert number is found to be so small that it leads to the decoupling of temperature effects on the mean flow motion. This confirms the routinely used assumptions made by previous investigators. In the present work, the small Péclet, moderate injection case is considered. Also, the use of the Dirac delta function to model the desired heat source displacement appears to be a viable artifact. The fair agreement with temperature maps in rocket motors provides the raison d'être for this basic formulation. In future work, the analysis may be extended to higher orders by fully incorporating the convective mean flow effects. Along similar lines, the heat source location may be adjusted by relating b to flame zone dynamics.

Acknowledgment

This project is sponsored, in part, by NSF grant No. CMS-0353518.

References

[1] Brewster, M. Q., 2000, *Solid Propellant Combustion Response: Quasi-Steady (QSHOD) Theory Development and Validation, Solid Propellant Chemistry, Combustion, and Motor Interior Ballistics*, V. Yang, T. B. Brill, and W.-Z. Ren, eds., AIAA Progress in Astronautics and Aeronautics, Washington, D.C., Vol. 185, pp. 607–637.
[2] T'ien, J. S., 1972, "Oscillatory Burning of Solid Propellants Including Gas Phase Time Lag," Combust. Sci. Technol., **5**, pp. 47–54.
[3] De Luca, L. T., 1992, *Theory of Nonsteady Burning and Combustion Stability of Solid Propellants by Flame Models, Nonsteady Burning and Combustion Stability of Solid Propellants*, L. T. De Luca, E. W. Price, and M. Summerfield, eds., AIAA Progress in Astronautics and Aeronautics, Washington, D.C., Vol. 143, pp. 519–600.
[4] Margolis, S. B., and Williams, F. A., 2000, *Structure and Stability of Deflagrations in Porous Energetic Materials, Solid Propellant Chemistry, Combustion, and Motor Interior Ballistics*, V. Yang, T. B. Brill, and W. Z. Ren, eds., AIAA Progress in Aeronautics and Astronautics, Washington, D.C., Vol. 185, pp. 549–590.
[5] Zemin, A. A., and Finjakov, S. V., 2000, *Burning Rate Response Functions of Composite-Modified Double-Base Propellants and HMX, Solid Propellant Chemistry, Combustion, and Motor Interior Ballistics*, V. Yang, T. B. Brill, and W. R. Ren, eds., AIAA Progress in Astronautics and Aeronautics, Washington, D.C., Vol. 185, pp. 639–662.
[6] Beddini, R. A., and Roberts, T. A., 1992, "Response of Propellant Combustion to a Turbulent Acoustic Boundary Layer," J. Propul. Power, **8**(2), pp. 290-296.
[7] Chedevergne, F., Casalis, G., and Feraille, T., 2006, "Biglobal Linear Stability Analysis of the Flow Induced by Wall Injection," Phys. Fluids, **18**(1), pp.

014103–014114.
[8] Griffond, J., and Casalis, G., 2001, "On the Nonparallel Stability of the Injection Induced Two-Dimensional Taylor Flow," Phys. Fluids, **13**(6), pp. 1635–1644.
[9] Apte, S., and Yang, V., 2001, "Unsteady Flow Evolution in a Porous Chamber With Surface Mass Injection. Part I: Free Oscillation," AIAA J., **39**(8), pp. 1577–1586.
[10] Majdalani, J., Barron, J., and Van Moorhem, W. K., 2001, "Experimental Classification of Turbulence in an Oscillatory Channel Flow With Transpiring Walls," *Proceedings ASME FEDSM 2001-1881*, New Orleans, LA, May 29–June 1, ASME, New York.
[11] Majdalani, J., Barron, J., and Van Moorhem, W. K., 2002, "Inception of Turbulence in the Stokes Boundary Layer over a Transpiring Wall," ASME J. Fluids Eng., **124**(9), pp. 1–7.
[12] Apte, S., and Yang, V., 2000, *Effect of Acoustic Oscillation on Flow Development in a Simulated Nozzleless Rocket Motor, Solid Propellant Chemistry, Combustion, and Motor Interior Ballistics*, V. Yang, T. B. Brill, and W.-Z. Ren, eds., AIAA Progress in Astronautics and Aeronautics, Washington, D.C., Vol. 185, pp. 791–822.
[13] Roh, T. S., Tseng, I. S., and Yang, V., 1995, "Effects of Acoustic Oscillations on Flame Dynamics of Homogeneous Propellants in Rocket Motors," J. Propul. Power, **11**(4), pp. 640–650.
[14] Roh, T. S., and Culick, F. E. C., 1995, "Transient Combustion Response of Homogeneous Propellants to Acoustic Oscillations in Axisymmetric Rocket Motors," *Proceedings AIAA 97-3325*, San Diego, CA, July 6–9.
[15] Venugopal, P., Najjar, F. M., and Moser, R. D., 2000, "DNS and LES Computations of Model Solid Rocket Motors," *Proceedings AIAA 2000-3571*, Huntsville, AL, July 16–19.
[16] Venugopal, P., Najjar, F. M., and Moser, R. D., 2001, "Numerical Simulations of Model Solid Rocket Motor Flows," *Proceedings AIAA 2001-3950*, Salt Lake City, UT, July 6–11.
[17] Vuillot, F., and Lupoglazoff, N., 1996, "Combustion and Turbulent Flow Effects in 2-D Unsteady Navier-Stokes Simulations of Oscillatory Rocket Motors," *Proceedings AIAA 96-0884*, Reno, NV, January 15–18.
[18] Vuillot, F., Dupays, J., Lupoglazoff, N., Basset, T., and Daniel, E., 1997, "2-D Navier-Stokes Stability Computations for Solid Rocket Motors: Rotational, Combustion and Two-Phase Flow Effects," *Proceedings AIAA 97-3326*, Seattle, WA, July 6–9.
[19] Reid, R. C., Prausnitz, J. M., and Poling, B. E., 1987, *The Properties of Gases and Liquids*, 4th ed., McGraw–Hill, New York.
[20] Culick, F. E. C., 1966, "Rotational Axisymmetric Mean Flow and Damping of Acoustic Waves in a Solid Propellant Rocket," AIAA J., **4**(8), pp. 1462–1464.
[21] Vuillot, F., 1995, "Vortex-Shedding Phenomena in Solid Rocket Motors," J. Propul. Power, **11**(4), pp. 626–639.
[22] Casalis, G., Avalon, G., and Pineau, J.-P., 1998, "Spatial Instability of Planar Channel Flow With Fluid Injection through Porous Walls," Phys. Fluids, **10**(10), pp. 2558–2568.
[23] Couton, D., Plourde, F., and Doan-Kim, S., 1999, "Analysis of Energy Transfers of a Sheared Flow Generated by Wall Injection," Exp. Fluids, **26**(3), pp. 222–232.
[24] Couton, D., Doan-Kim, S., and Vuillot, F., 1997, "Numerical Simulation of Vortex-Shedding Phenomenon in a Channel With Flow Induced through Porous Wall," Int. J. Heat Fluid Flow, **18**(3), pp. 283–296.
[25] Couton, D., Plourde, F., and Doan-Kim, S., 1996, "Cold Gas Simulation of a Solid Propellant Rocket Motor," AIAA J., **34**(12), pp. 2514–2522.
[26] Chu, W.-W., Yang, V., and Majdalani, J., 2003, "Premixed Flame Response to Acoustic Waves in a Porous-Walled Chamber With Surface Mass Injection," Combust. Flame, **133**(6129), pp. 359–370.
[27] Vyas, A. B., Majdalani, J., and Yang, V., 2003, "Estimation of the Laminar Premixed Flame Temperature and Velocity in Injection-Driven Combustion Chambers," Combust. Flame, **133**(6129), pp. 371–374.
[28] Roh, T. S., Apte, S., and Yang, V., 2000, *Combustion Dynamics of Homogeneous Solid Propellants in a Rocket Motor With Acoustic Excitations, Solid Propellant Chemistry, Combustion, and Motor Interior Ballistics*, V. Yang, T. B. Brill, and W.-Z. Ren, eds., AIAA Progress in Astronautics and Aeronautics, Washington, D.C., Vol. 185, pp. 885–906.